Journal of Materials Science and Chemical Engineering, 2026, 14(4), 31-52
https://www.scirp.org/journal/msce
ISSN Online: 2327-6053
ISSN Print: 2327-6045

Physico-Chemical, Mineralogical, and Morphological Characterizations of Three Clays from Côte d'Ivoire with a View to Their Use in Adsorption

Bi Gamy Arsène Tra[1,2*], Drissa Bamba[2], Namory Méité[1], Alfred Niamien Kouamé[1], Mariame Coulibaly[2], Koffi Léon Konan[1]

[1]Université Félix Houphouët-Boigny (UFHB), UFR SSMT, Laboratoire de Constitution et Réaction de la Matière (LCRM), Abidjan, Côte d'Ivoire
[2]Ecole Normale Supérieure (ENS), Laboratoire des Sciences Physiques Fondamentales et Appliquées (LSPFA), Abidjan, Côte d'Ivoire
Email: *arsenetrabi86@gmail.com

How to cite this paper: Tra, B.G.A., Bamba, D., Méité, N., Kouamé, A.N., Coulibaly, M. and Konan, K.L. (2026) Physico-Chemical, Mineralogical, and Morphological Characterizations of Three Clays from Côte d'Ivoire with a View to Their Use in Adsorption. *Journal of Materials Science and Chemical Engineering*, **14**, 31-52.
https://doi.org/10.4236/msce.2026.144003

Received: March 12, 2026
Accepted: April 24, 2026
Published: April 27, 2026

Abstract

This study focuses on the physicochemical, mineralogical, and morphological characterization of three natural clays from Côte d'Ivoire (KR, KB, and BB) to evaluate their potential for environmental applications. The samples were analyzed by particle size analysis, X-ray fluorescence (XRF), X-ray diffraction (XRD), FTIR spectroscopy, scanning electron microscopy (SEM/EDS), and thermal analysis. The results show a predominance of kaolinite in KR and BB, while KB exhibits a more diverse mineralogy including illite and smectite. Iodine values (593.55 mg/g for KR, 511.50 mg/g for KB, and 505.03 mg/g for BB) and methylene blue values close to 320 - 330 mg/g indicate differences in the textural properties and accessible surface area of the materials. These results highlight the superior adsorption potential of KR, linked to its high kaolinite and iron oxide content, while KB exhibits promising potential due to its smectite fraction. This study thus provides an essential database for selecting local clay materials that could be further investigated in water treatment applications.

Keywords

Natural Clays, Adsorption, Iodine Value, Methylene Blue Value, Pollution Remediation, Côte d'Ivoire

1. Introduction

Clays are abundant, finely divided natural materials, primarily composed of hy-

drated aluminum silicates. Their lamellar crystalline structure, resulting from the stacking of tetrahedral (SiO_4) and octahedral (AlO_6) sheets, gives these minerals remarkable physicochemical properties such as a high specific surface area, developed porosity, significant cation exchange capacity, and notable plasticity [1] [2]. These structural characteristics promote interactions between the clay surface and various chemical species, making clays particularly well-suited for environmental applications. The effectiveness of clays in wastewater treatment is primarily linked to these structural and physicochemical properties, including specific surface area, cation exchange capacity, surface charge, and the nature of the clay sheets. Adsorption mechanisms generally involve several complementary processes such as ion exchange, physical adsorption, surface complexation, and electrostatic interactions. These mechanisms are highly dependent on the mineralogical structure and chemical reactivity of the clay surfaces, which control the nature of the adsorbent-adsorbate interactions and the pollutant removal performance in wastewater treatment systems [3]-[5].

In a context marked by the intensification of industrial and agricultural activities, the contamination of water resources by synthetic dyes, heavy metals, and excess nutrients constitutes a major environmental issue. Given the economic and technical limitations of certain conventional water treatment technologies, the use of local, low-cost natural materials is generating increasing interest. Clays thus stand out as promising adsorbents due to their availability, chemical stability, and demonstrated effectiveness in removing many pollutants [6] [7].

However, the adsorption performance of clays is highly dependent on their mineralogical and chemical composition. The main clay phases, such as kaolinite, illite, and smectites, particularly montmorillonite, exhibit differentiated behaviors due to their respective crystalline structures and surface properties. Smectite-type minerals generally display a high adsorption capacity due to their expansive 2:1 structure and their high cation exchange capacity linked to isomorphic substitutions in the crystal lattice. Conversely, kaolinite, characterized by a more stable and less charged 1:1 structure, generally exhibits a more moderate adsorption capacity but high chemical inertness [8] [9]. Moreover, the presence of accessory minerals such as iron oxides can influence interaction mechanisms through complexation or electrostatic attraction [10] [11].

In Côte d'Ivoire, clay resources are abundant and widely distributed throughout the territory, but their utilization in the field of water depollution is still insufficiently developed. Although some studies have highlighted the potential of these materials for the adsorption of dyes and toxic metals [6] [12] [13], the relationships between mineralogical composition, physico-chemical properties, and adsorptive efficiency are still poorly documented in a systematic manner.

This study aims to characterize three clay samples collected in Côte d'Ivoire by analyzing their mineralogical composition and physicochemical properties, and then evaluating their adsorption potentials. The objective is to establish correlations between the dominant mineral phases and the observed potentials, in order

to contribute to the development of local, sustainable, and economically accessible solutions for water pollution control.

2. Materials and Methods

2.1. Sampling Sites and Samples

Three clay samples from different regions of Côte d'Ivoire (West Africa) were studied. One sample was taken from Bongouanou, in the Moronou region (Central-East), labeled BB, and two samples were collected from Katiola, in the Hambol region (North), designated KR and KB. Samples KR and KB were collected from two separate sites in the Katiola area to ensure better spatial representation. The clays studied originate primarily from lateritic formations resulting from the weathering of crystalline rocks of the Birimian basement. These formations are the result of intense tropical weathering processes that promote the formation of secondary minerals such as kaolinite, iron oxides and oxyhydroxides, and quartz [14]. The Katiola region belongs to the geological domain of north-central Côte d'Ivoire, characterized by highly weathered granitoid formations [15]. In contrast, the Bongouanou area is located in an internal sedimentary basin dominated by clayey-sandy formations [16]. Samples were collected at depths of 0 to 20 cm using a hoe. For each site, three subsamples were collected and then homogenized to create a representative composite sample. The materials were packaged in 15 kg nylon bags without prior treatment. Before characterization, the samples were air-dried in the shade for several days, crushed, disaggregated, and then finely ground in an agate mortar. The resulting powders were sieved at 63 µm to ensure a homogeneous particle size suitable for analysis. Photographs of the studied clays are presented in **Figure 1**.

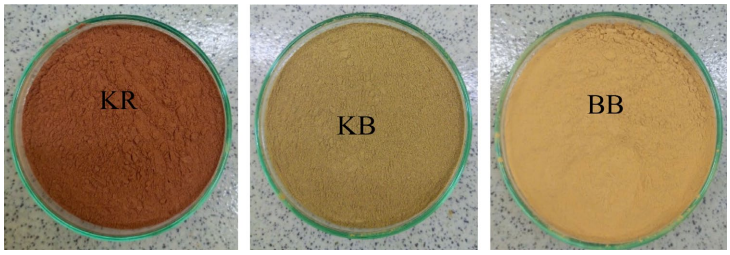

Figure 1. Images of the clay samples.

2.2. Methods of Characterizing Clay Samples

All experimental analyses were performed in triplicate to ensure the reproducibility of the results. The values presented in the tables correspond to the arithmetic means with their standard deviations. This approach allows for the evaluation of the analytical precision and experimental variability of the physicochemical measurements.

2.2.1. Physical Characterization

The moisture content of the clays was determined according to standard NF P 94-

050 [17] by evaluating the mass loss after drying the samples in an oven at 105˚C for 24 hours. The moisture content is expressed as a percentage of the dry mass and is determined by Equation (1)

$$\mathrm{TH}(\%)=\frac{(m_1-m_2)\times 100}{m_1} \tag{1}$$

m_1 (g): mass of the raw sample; m_2 (g): mass of the sample after drying at 105˚C for 24 hours in an oven.

The loss on ignition was obtained after calcination at 1000˚C for 2 hours in the furnace of samples previously dried in the oven at 105˚C [18] [19]. The loss on ignition is calculated according to the formula given by Equation (2):

$$\mathrm{PF}(\%)=\frac{(m_2-m_3)\times 100}{m_2} \tag{2}$$

m_2 (g): mass of the sample after drying at 105˚C for 24 hours; m_3 (g): mass of the sample after calcination at 1000˚C for 2 hours in a furnace.

The protocol used to measure pH is that of Khireddine [20]. Contact is established between the powdered clay and distilled water or a KCl solution (1 mol/L) in a ratio (m/V = 1/5) for the determination of pH (H_2O) and pH (KCl), respectively. Contact is maintained using magnetic stirring for 1 hour. After 2 hours of resting, the pH measurement is carried out in the supernatant using a pH meter. The organic matter (OM) content was determined according to the hydrogen peroxide method [21], which consists of treatment with hydrogen peroxide, 10 volumes (H_2O_2, 3%), of the material as described by Laibi *et al.* [22]. The organic matter content is calculated using the formula given by Equation (3):

$$\mathrm{MO}(\%)=\frac{(m_0-m_1)\times 100}{m_0} \tag{3}$$

m_0 (g): initial mass of the clay sample before the reaction with hydrogen peroxide; m_1 (g): mass of the sample after the reaction and oven-dried at 105˚C for 24 hours.

The density of clay materials was determined using the water pycnometer method according to the protocol described by Gagea and Mirica [23]. The value of the sample density is given by Equation (4):

$$\rho=\left[\frac{(m_2-m_1)\times(\rho_L-\rho_a)}{m_4(m_2-m_1)-m_3}\right]+\rho_a \tag{4}$$

ρ (g·cm^{-3}): density of clay; ρ_L (g·cm^{-3}): density of water (1 g·cm^{-3}); ρ_a (g·cm^{-3}): density of air (0.0012047 g·cm^{-3}); m_1 (g): mass of the empty pycnometer; m_2 (g): mass of the pycnometer with 5 g of clay; m_3 (g): mass of the pycnometer with the same amount of clay and filled with distilled water; m_4 (g): mass of the pycnometer filled with distilled water.

2.2.2. Chemical Composition

The chemical composition in oxides of the clay samples was determined by X-

ray fluorescence spectrometry (XRF), using an energy-dispersive spectrometer (EDXRF) model PANalytical Epsilon 4 at the Analysis and Research Center of PETROCI in Côte d'Ivoire. The analyses were carried out on finely ground and homogenized powders, allowing the quantification of the main major and minor oxides present in the samples. This non-destructive technique offers a precise and rapid determination of the overall elemental composition of the materials.

2.2.3. X-Ray Diffraction

The mineralogical composition of the clays was determined by powder X-ray diffraction (XRD) using a powder X-ray diffractometer (Rigaku Miniflex) operating at 30 kV and 15 mA at the National Geosciences Research Laboratory (NGRL), Kaduna, Nigeria.

These PXRD analyses were carried out using monochromatic CuKα radiation ($\lambda = 1.54056$) with a measurement range in 2θ from 4˚ to 75˚. The mineral phases were identified using HighScore software and a PDF (powder diffraction files) database from the ICDD (International Center for Diffraction Data).

2.2.4. Fourier Transform Infrared Spectroscopy of Clays

Infrared absorption spectra were obtained with an Agilent Cary 630 FTIR Fourier transform spectrometer, scanning from 4000 to 650 cm^{-1}. The analysis was conducted at the Laboratory of Chemistry and Renewable Energies (LaCER) of the Nazi BONI University, Bobo-Dioulasso, Burkina Faso.

2.2.5. Morphological and Microstructural

Analysis Scanning electron microscopy coupled with energy-dispersive X-ray spectroscopy (SEM/EDS) was performed using a Phenom ProX electron microscope (ProX, Netherlands).

The analysis was carried out at the National Geosciences Research Laboratory (NGRL), Kaduna, Nigeria.

2.2.6. Differential Thermal Analysis and Thermogravimetry (DTA/TGA)

Thermal analysis aims to characterize materials by studying their properties or changes in state as a function of temperature and time. The main techniques used are differential thermal analysis (DTA) and thermogravimetry (TGA). The analysis was conducted at the National Geosciences Research Laboratory (NGRL), Kaduna, Nigeria, using a PerkinElmer TGA 4000 made in Netherlands.

2.2.7. Adsorptive Properties

The iodine number was determined according to the procedure established by the American Society for Testing and Materials (ASTM D4607). The contact time between the clay and the iodine solution was set at 30 minutes under constant stirring (200 rpm) at 25˚C before titration with 0.1 N sodium thiosulfate. The experimental reproducibility is estimated at ± 2 $mg{\cdot}g^{-1}$. The concentration of iodine adsorbed by clay materials (Iodine Index) was calculated as the amount of iodine adsorbed in milligrams using Equation (5) [24] [25].

$$Id = \frac{(V_b - V_s) \times M \times N \times 10}{M \times V_b} \quad (5)$$

With: V_b (mL): volume of sodium thiosulfate added during the blank test (without clay); V_S (mL): volume of sodium thiosulfate added during the test with clay; N (mol/L): normality of the iodine solution; m (g): mass of the clay; M (g/mol): molecular mass of diiodine (253.81 g/mol).

Agitation was carried out at 200 rpm for 30 h at 25˚C.

The protocol used for the determination of the methylene blue index is the one reported by Bestani *et al.* [26]. First, a mass of 0.3 g of clay is mixed with 100 mL of 1000 mg/L methylene blue solution. After 24 hours of agitation at 25˚C, the suspension was filtered and the residual concentration of methylene blue was measured using a UV/VIS spectrophotometer (Jasco V530 UV/Vis) at a wavelength of 664 nm [27] with a precision of ± 0.005 absorbance units. The methylene blue adsorption capacity (IBM) is given by Equation (6)

$$\text{IMB} = \frac{(C_i - C_r) \times V}{m} \quad (6)$$

With: C_i and C_r: the initial and residual concentrations of methylene blue (in g/L); V: volume (in L) of the methylene blue solution used for adsorption tests and m: the mass (in g) of the clay.

The pH at the point of zero charge (pH_{PZC}) was determined by the method reported by Kouakou *et al.* [6]. A volume of 40 mL of NaCl (0.1 M) was introduced into Erlenmeyer flasks containing 0.2 g of the clay to be analyzed. The pH of each Erlenmeyer flask was adjusted in the range of 2 to 12 by adding a 0.1 M HCl or 0.1 M NaOH solution. The Erlenmeyers were covered and stirred for 72 hours at a temperature of 25˚C. After stirring, the contents of these Erlenmeyer flasks were filtered through 0.45 µm filter paper. The final pH of each mixture was measured using a pH meter. The graph of pH variation versus initial pH was plotted. The pH_{PZC} is defined as the point of intersection of the curve with the zero axis ΔpH = 0 [6] [27].

Particle size analysis was performed using a combination of mechanical sieving for coarse fractions and the Robinson pipette method for fine fractions. The pipette method, based on the principle of particle sedimentation according to Stokes' law, is recognized as a reference technique for the accurate determination of fine soil fractions [28]. The particle size classes used were: Clay: <2 µm; Fine silt: 2 - 20 µm; Coarse silt: 20 - 50 µm; Sand: >50 µm

3. Results and Discussion

3.1. Physical Characterizations

The results of the physico-chemical parameters of the clay samples are presented in **Table 1**.

Particle size distribution constitutes a determining parameter in adsorption phenomena, as it directly affects the available specific surface area and the number

of accessible active sites. The clay fraction is generally recognized as the most reactive, due to its fineness and high surface activity [29]. In the present study, the samples exhibit relatively low to moderate clay contents (4.5% - 7%), suggesting a limited contribution of this fraction to the overall adsorption capacity. Fine silt, particularly abundant in the KR sample (61%), may participate in adsorption mechanisms, although its effectiveness remains lower than that of clay particles. Conversely, the sandy fraction, which is minor and chemically less reactive, plays a negligible role in adsorption processes.

Table 1. Main physico-chemical properties of the clay samples.

Parameters	KR	KB	BB
Clay fraction (%)	5.5	7.0	4.5
Fine silt (%)	61.0	41.0	30.5
Coarse silt (%)	25.9	44.4	50.25
Sand (%)	7.6	6.0	6.75
Moisture content (%)	1.41 ± 0.02	1.38 ± 0.16	0.27 ± 0.02
pH (H_2O)	6.43 ± 0.1	6.40 ± 0.13	6.14 ± 0.2
pH (KCl)	4.51 ± 0.14	6.00 ± 0.1	4.00 ± 0.2
Density ($g \cdot cm^{-3}$)	2.48 ± 0.03	2.44 ± 0.02	2.66 ± 0.01
Organic matter (%)	1.36 ± 0.08	1.92 ± 0.06	0.58 ± 0.1

The moisture content (HR) is a determining factor in the mechanisms of interaction between pollutants and the soil matrix, by providing an aqueous interface favorable to adsorption phenomena. The KR and KB samples, with moisture contents above 1%, thus have an environment more conducive to contaminant retention, compared to the BB soil, whose lower HR (0.27%) limits the effectiveness of physicochemical interactions between pollutants and adsorption sites. Values close to those obtained in the present study have been reported in other works: 2.71 - 2.72 [30], 1.12% ± 0.5% - 3.98% ± 0.4% [25], and 3.53% [31]. However, they remain lower than those reported by [22] [32], which are respectively 3.71% ± 0.1% - 4.54% and 4.78%.

Density measurements with the water pycnometer gave values of 2.48; 2.44 and 2.66 $g \cdot cm^{-3}$ for the KR, KB, and BB samples, respectively. These values fall within the density ranges reported for clay minerals, namely: 2.0 - 2.6 $g \cdot cm^{-3}$ for smectites, 2.61 - 2.68 $g \cdot cm^{3}$ for kaolinites, and 2.6 - 3.3 $g \cdot cm^{-3}$ for chlorites [33]. The density of KR and KB suggests a dominance of smectite phases, while that of BB corresponds to the characteristic values of kaolinites and to the lower limit of chlorites. Density values alone do not allow us to conclude that smectites are dominant. Reliable mineralogical identification relies primarily on XRD results, which indicate a dominance of kaolinite in KR [34].

The pH measured in water (pH_{H2O}) and in a KCl solution (pH_KCl) allows for the estimation of the electrostatic adsorption potential of soils. The difference between these two values, called ΔpH (pH_{H2O}-pH_KCl), provides information on the net surface charge: a positive ΔpH indicates a negatively charged surface, favorable for the adsorption of cationic organic pollutants. The ΔpH values measured for the KR and BB samples, exceeding +1.9, reflect a predominance of negative charges on the particle surfaces, indicating a strong affinity for cationic species through electrostatic adsorption mechanisms. In contrast, the KB sample shows a significantly lower ΔpH (+0.4), suggesting a reduced density of negative charge and, therefore, a lower electrostatic adsorption capacity. However, this limitation is largely offset by a notable organic matter content (1.92%), which plays a central role in the adsorption of organic compounds. Organic matter indeed acts as an effective adsorptive phase, through hydrophobic interactions, Van der Waals forces, and π-π bonding, which are particularly important in soils with low clay content. This crucial role of organic matter in the retention of organic pollutants is supported by the work of Ewis *et al.* [35], who highlight its significant contribution to surface charge and overall retention capacity, especially in the context of low fine mineral fraction. Furthermore, the work of Claudia *et al.* demonstrated that ΔpH is a good indicator of cationic adsorption capacity, directly related to the soil's organic carbon content [36].

3.2. Chemical Composition of the Clay Samples

The chemical composition of the three clay samples, presented in **Table 2**, highlights the main constituent oxides. X-ray fluorescence analyses show that silica (SiO_2) is the major oxide in all three samples, with contents ranging from 46.17% (KR) to 58.09% (BB). Alumina (Al_2O_3) varies from 17.24% (KB) to 21.91% (KR), confirming the dominance of aluminosilicates. The KR sample stands out for its high Fe_2O_3 content (16.85%), significantly higher than that of KB (9.26%) and BB (3.68%), indicating a marked iron enrichment. Alkali oxides (K_2O and Na_2O) are higher in KB (1.67% and 1.21%), suggesting a more significant contribution of potassium or sodium phases. KB also shows the highest content of MgO (1.90%) and CaO (1.23%).

The SiO_2/Al_2O_3 ratio ranges from 2.10 (KR) to 2.89 (KB and BB), indicating a relatively more aluminous composition for KR and more siliceous for KB and BB. The loss on ignition (LOI) ranges between 5.25% (KB) and 10.24% (BB), reflecting the presence of structural water and possible hydrated phases. The red and yellow colors observed respectively in KR, KB, and BB indicate the presence of oxidized iron (Fe^{3+}) [37] [38]. The mass ratios SiO_2/Al_2O_3 of the KR, KB, and BB samples are respectively 2.13 - 2.85 and 2.93. These mass ratios, ranging between 2 and 4, show that these three samples are mainly composed of 2:1 type mineral. Indeed, according to Konan [39], the SiO_2/Al_2O_3 mass ratio of 2:1 type materials range between 2 and 4. Although the SiO_2/Al_2O_3 ratios might suggest the presence of 2:1 minerals, the XRD results clearly indicate a dominance of kaolinite in KR and BB.

This apparent contradiction can be explained by the presence of free quartz, albite, or other non-clay silicate phases that artificially increase the silica content without altering the dominant clay mineralogy [40].

Table 2. Mass % composition of oxides in KR, KB, and BB clays.

Oxides (wt%)	KR	KB	BB
SiO_2	46.7	49.2	58.9
Al_2O_3	21.91	17.24	20.07
Fe_2O_3	16.85	9.26	3.68
K_2O	0.86	1.67	1.49
Na_2O	0.17	1.21	0.31
MgO	1.16	1.90	0.20
Organic matter (%)	0.02	0.06	0.00
TiO_2	1.03	0.76	0.69
CaO	0.04	1.23	0.00
P_2O_5	0.04	0.07	0.03
LOI (Loss on ignition)	9.00	5.25	10.24
SiO_2/Al_2O_3 ratio	2.10	2.89	2.89

3.3. X-Ray Diffraction

Figure 2 shows the X-ray diffraction (XRD) pattern of the raw clays.

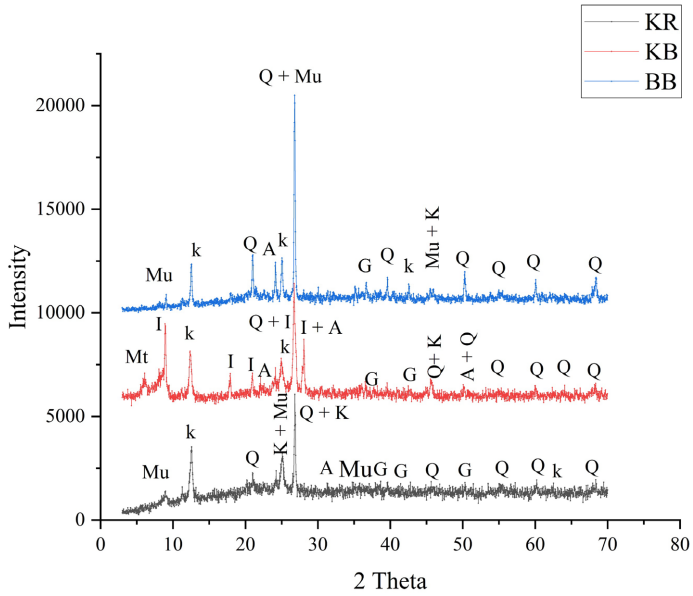

Figure 2. XRD patterns of raw clays (fraction = 63 μm): Quartz (Q), Kaolinite (K), Albite (A), Muscovite (Mu), Goethite (G), Illite (I) and Montmorillonite (Mt)

In the three spectra, the characteristic peaks of kaolinite appear at 7.16 Å (2θ = 12.35˚) and at 3.55 Å (2θ = 25.05˚). The presence of goethite was also detected in all three samples, with a peak located at 2.45 Å (2θ = 36.6˚). Albite is identified by a peak at 3.68 Å (2θ = 24.13˚). Other non-clay minerals, considered as impurities, are also present. Thus, for the KR, BB, and KB samples, quartz is highlighted by peaks at 4.23 Å (2θ = 20.96˚) and at 3.33 Å (2θ = 26.75˚). The XRD spectrum of the KB sample additionally reveals the presence of illite, identified by peaks at 9.83 Å (2θ = 8.98˚), 4.95 Å (2θ = 17.90˚), and 4.23 Å (2θ = 20.95˚), as well as montmorillonite, detected by a peak at 14.18 Å (2θ = 6.23˚). Finally, muscovite is identified in the KR and BB samples, with a peak located at 9.92 Å (2θ = 8.91˚).

3.4. Mineralogical Composition

The mineral proportions were estimated using a semi-quantitative approach based on the relative intensity of the characteristic peaks of the phases identified on the XRD diffractograms. (Table 3). Kaolinite is the main clay mineral in both the KR and BB samples, with proportions ranging between 37.20% and 47.63%, while montmorillonite is the main mineral of KB. All clays also contain albite and goethite (between 1.44% and 10.23%; 4.09% and 18.75%, respectively), whereas montmorillonite and illite were detected only in the KB sample, where they reach 24.71% and 14.82%, respectively. The low goethite content (4.0%) in the BB1 sample explains its white color.

Table 3. Mineralogical percentages of the clays.

Samples	% Albite	% Goethite	% Muscovite	% Montmorillonite	% Kaolinite	% Illite	% Quartz
KR	1.44	18.75	7.28	-	47.63	-	19.73
KB	10.23	10.3	-	24.71	10.65	14.82	15.73
BB	2.62	4.09	12.62	-	37.20	-	33.28

Numerous studies have shown that montmorillonite-type clays have high specific surface areas as well as significant cation exchange capacity, giving them adsorption performance that is markedly superior to that of kaolinites [8] [41] [42]. This difference is mainly attributed to their 2:1 type crystal structure, characterized by isomorphic substitutions within the tetrahedral and octahedral sheets, generating a permanent negative charge compensated by exchangeable cations (Na^+, Ca^{2+}, Mg^{2+}). Furthermore, the presence of iron oxyhydroxides, notably goethite, significantly contributes to the enhancement of the adsorptive properties of clay matrices [3]. The work of Aké *et al.* [7] thus observed that kaolinites rich in goethite exhibit an increased phosphate adsorption capacity.

Moreover, the presence of iron oxyhydroxides, notably goethite, contributes significantly to the improvement of the adsorptive properties of clay matrices [6]. The work of Aké *et al.* [7] showed that kaolinites enriched with goethite exhibit an increased phosphate adsorption capacity, due to the strong affinity of the sur-

face hydroxyl groups of iron for oxygen-containing anions. The adsorptive performance observed in the studied samples results from the synergistic action of several complementary mechanisms. Ion exchange constitutes a major mechanism, particularly pronounced in the KB sample containing 24.71% montmorillonite. The permanent negative charges resulting from isomorphic substitutions are compensated by exchangeable interlayer cations. In aqueous solution, these cations can be replaced by dissolved metal species, which explains the high cation retention capacity observed for this sample [43].

Electrostatic interactions depend closely on the pH of the medium and the pH at the zero-charge point (pH_{ZCP}). When the pH is higher than the pH_{ZCP}, the surface of the adsorbent acquires an overall negative charge, promoting the adsorption of cationic species through electrostatic attraction. Conversely, when the pH is lower than the pH_{ZCP}, the surface becomes overall positive, which favors the binding of anions. This mechanism mainly occurs in the non-specific retention of ionic species [44]. Finally, in the KR sample, characterized by a high content of Fe_2O_3 (16.85%) and goethite (18.75%), surface complexation plays a decisive role. The hydroxyl groups of iron oxides and oxyhydroxides participate in coordination reactions with dissolved species, according to a general type of mechanism:

$$\equiv Fe-OH + M^{2+} \rightarrow \equiv Fe-OM^{+} + H^{+}$$

This process leads to the formation of inner-sphere complexes, reflecting a more specific and stable binding of metal cations as well as oxygen-containing anions, notably phosphate. Unlike purely electrostatic interactions, these bonds involve electron sharing and confer greater thermodynamic stability to the adsorbed species [45]. Ultimately, the adsorptive efficiency of the studied materials is closely controlled by their mineralogical and chemical composition. Montmorillonite mainly promotes ion exchange and electrostatic adsorption, while the presence of ferriferous phases such as goethite enhances specific binding through surface complexation. The complementarity of the physico-chemical mechanisms involved could explain the differences in adsorption potential observed between the KB and KR samples [43] [46].

3.5. Morphological and Microstructural Analysis

The images of KR, KB, and BB clays are shown in **Figure 3**. Analyses reveal the presence of kaolinite, identified in the form of stacked pseudo-hexagonal platelets [47]-[50], often disordered, particularly in iron-rich samples. This morphology is typical of poorly crystalline kaolinites, but also of illites [51] [52]. Furthermore, notable amounts of swelling minerals, such as montmorillonite, as well as quartz, have also been confirmed. Images from electron microscopy show fine aggregates and rods with irregular contours, illustrating the complexity and diversity of the assemblages present in these clay materials. These results provide important insight into the nature and potential of local clay resources.

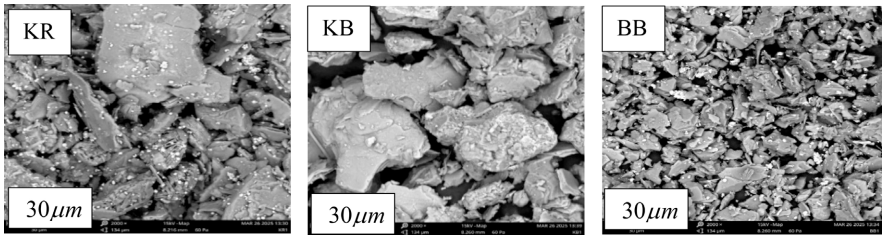

Figure 3. Scanning electron microscopy of KR, KB, and BB clays.

EDS analysis confirmed the chemical composition of the samples (**Table 4**), dominated by silicon and aluminum, elements characteristic of phyllosilicates. However, the KR sample stands out for its high iron content (17.90%), which enhances its capacity to complex certain organic pollutants. The KB sample, on the other hand, shows an enrichment in exchangeable cations (K, Ca, Mg, Na), promoting physicochemical interactions with molecules. These observations are consistent with the results of Bohm *et al.*, who demonstrated that the nature of exchangeable cations in phyllosilicates strongly influences the adsorption of hydrophobic organic pollutants such as hexachlorobenzene (HCB) [53]. In contrast, BB, although rich in silicon, exhibits low contents of iron, magnesium, and organic matter, reflecting a relatively inert structure. Thus, the comparison of granulometric, physico-chemical, and elemental data highlights the generally superior adsorbent potential of KR, followed by KB. BB appears to be the least effective, due to its low surface activity and a poorly reactive mineralogy.

Table 4. EDS analysis of the atomic composition of clays.

Samples	Si	Fe	Al	K	Ti	Mg	Mn	Na	Ca
KR	48.21	17.90	28.16	2.40	1.23	1.66	0.25	0.20	0.00
KB	53.21	13.16	22.38	3.73	0.89	2.99	0.00	1.79	1.85
BB	61.42	9.32	24.28	4.47	0.41	0.00	0.00	0.00	0.09

3.6. Thermal Analyses

The thermal analysis curves of the three samples (BB, KB, and KR) shown in **Figure 4** display similar profiles.

On the derivative thermogravimetry (DTG) curves, two major peaks are observed: The first peak, located between 25˚C and 200˚C, is attributed to the loss of hygroscopic water, consisting of water molecules adsorbed on the surface of the minerals [54] [55]. The release of this water does not cause any modification of the crystalline structure of the material [56]. The second peak, located around 400˚C, corresponds to the dehydroxylation of kaolinite. This dehydroxylation leads to the formation of metakaolinite, according to the chemical reaction [57].

$$Si_2Al_2O_5(OH)_4 \rightarrow Si_2Al_2O_7 + 2H_2O$$

SEM observations show that the surfaces of the samples are made up of aggre-

gates of clay sheets with a pseudo-hexagonal shape, exhibiting various degrees of alteration. EDS analysis indicates a high iron content on the surface, which could favor the rapid dehydroxylation of kaolinite into metakaolinite around 400˚C. These results suggest that the chemical composition and morphology of the sheets directly influence the thermal behavior of clays. Recent studies indicate that the dehydroxylation of kaolinite begins at temperatures of about 350˚C, 400˚C, 450˚C and continues up to 500˚C, 600˚C, which is consistent with our experimental results [58]. These two phenomena result in significant mass losses on thermogravimetric analysis (TGA) curves, indicating the main stages of dehydration and clay de-structuring during heating.

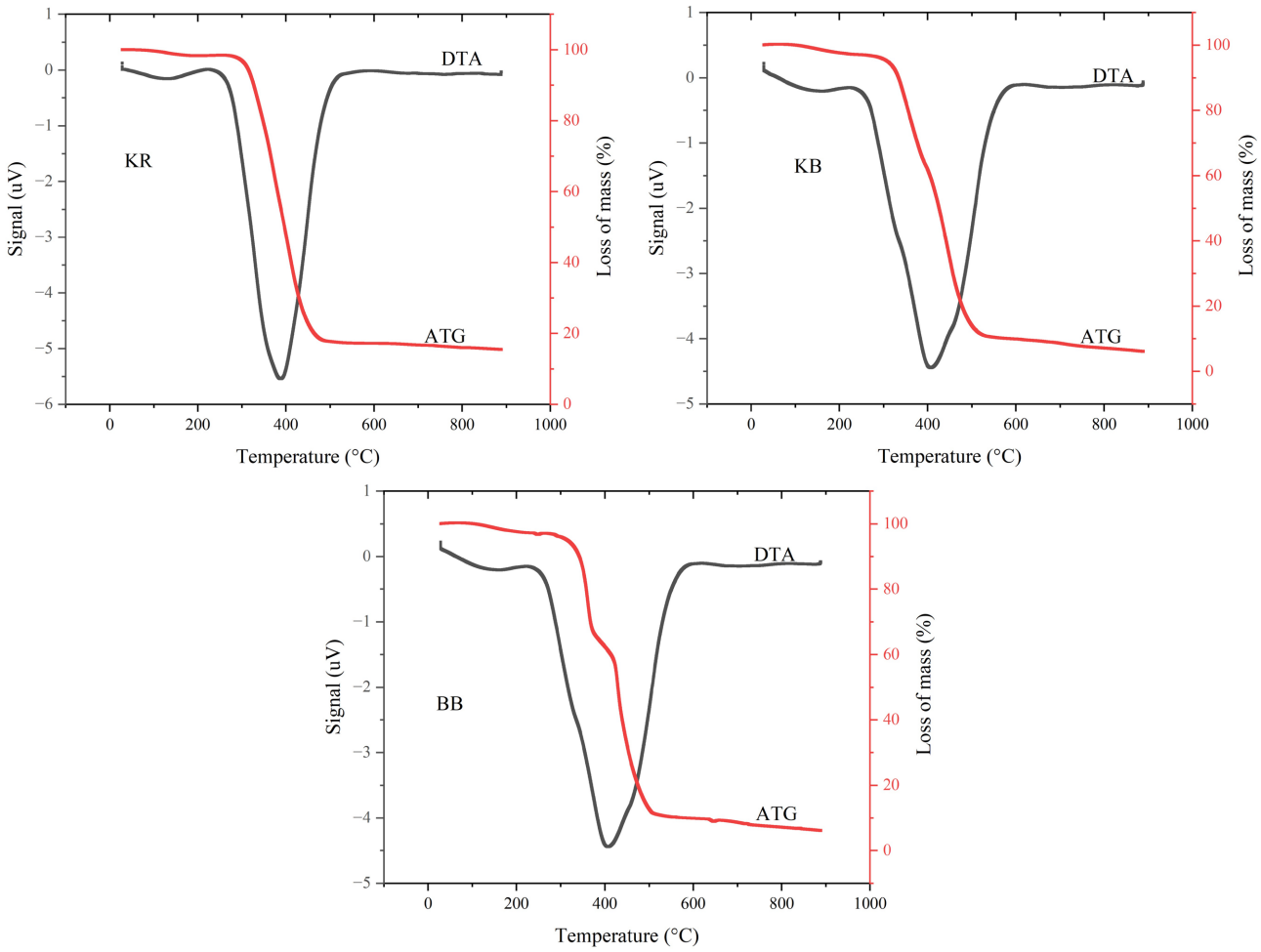

Figure 4. Thermograms (TGA and DTG curves) of the KR, KB, and BB.

3.7. Fourier Transform Infrared Spectroscopy

The analyses were carried out in the wavenumber range from 600 to 4000 cm^{-1}. The main bands observed in the spectra are shown in **Figure 5**.

The Fourier-transform infrared (FTIR) spectra of the KR and BB samples reveal similar spectral profiles. In the high-frequency region (3500 - 4000 cm^{-1}), three weak bands are observed at 3690, 3649, and 3619 cm^{-1}, while the KB sample shows

two bands located at 3697 and 3620 cm^{-1}. These bands are characteristic of the stretching vibrations of the structural hydroxyl groups (−OH) of kaolinite, according to the assignments proposed by Victor *et al.* [59]. The bands at 3690 - 3697 cm^{-1} and 3649 cm^{-1} are associated with the so-called external hydroxyls, located in the interlayer space, while the one at 3619 cm^{-1}, common to all samples, corresponds to internal hydroxyls linked to the central octahedral plane of kaolinite [60].

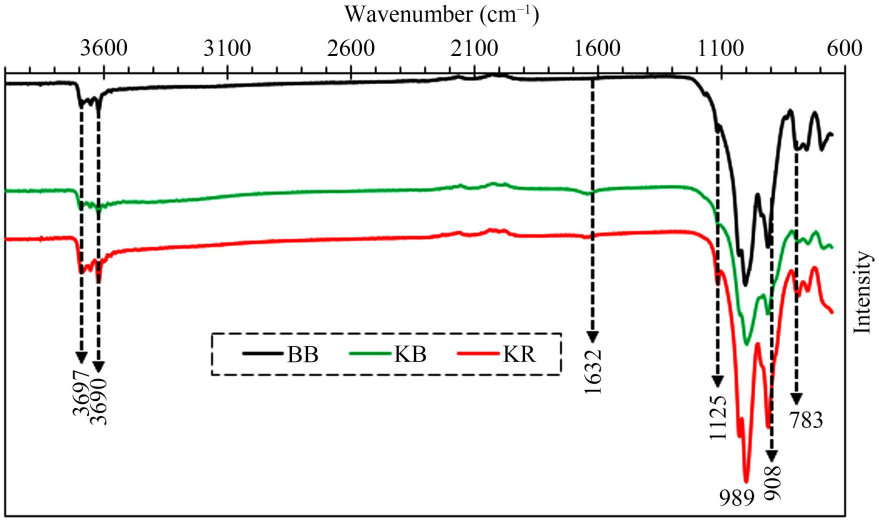

Figure 5. IR spectra of BB, KB, and KR.

In the intermediate region (700 - 1800 cm^{-1}), the spectra reveal bands related to the vibrations of the tetrahedral SiO_4 network, the deformations of hydroxyl groups, and adsorbed water [61]. Medium-intensity bands appear at 685, 735 - 754, and 783 - 791 cm^{-1}, typical of kaolinite-type clays, and attributed to vibrations of OH perpendicular to the surface or to translational movements [47] [60]. A strong band at 908 cm^{-1}, common to all three samples, indicates the deformation vibration of internal Al_2OH groups [60]. Bands observed at 1622 cm^{-1} for KB and at 1632 cm^{-1} for KR and BB correspond to the deformation vibrations of OH from adsorbed water [6]. Finally, the strong bands recorded at 989, 998, 1007, 1021, 1025, 1106, and 1125 cm^{-1} correspond to the stretching vibrations of Si-O bonds, relating to the silicate structure of the clays [61].

3.8. Adsorption Properties

The pH at the zero-charge point (pH_{ZCP}) of the adsorbents, corresponding to the pH at which the net surface charge is zero, was determined by identifying the intersection of the curves of initial and final pH variation (**Figure 6** and **Table 5**). The obtained values are 6.1 for KR, 5.3 for KB, and 5.4 for BB. This parameter is influenced by the nature of the functional groups present on the surface of the samples. When the pH of the medium is below the pH_{ZCP} ($pH < pH_{ZCP}$), the surface of the adsorbent is positively charged, thereby promoting the attraction of anionic

pollutants to the surface of the adsorbent [62], and when the pH of the solution is above the pH_{ZCP} ($pH > pH_{ZCP}$), the surface of the adsorbent is negatively charged, which promotes the attraction of cationic pollutants to the surface of the adsorbent [51] [63].

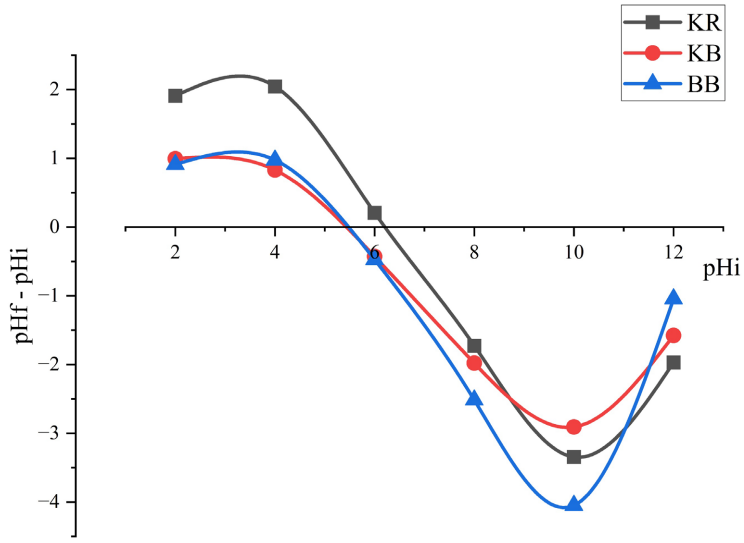

Figure 6. Effect of the variation of the pH of the aqueous solution on KR, KB, and BB clays.

The methylene blue index is another parameter commonly used to evaluate the adsorption capacity of materials. This parameter is related to the macro- and mesopore capacity of the material [64] [65]. This index defines the large pores (<50 nm) and is used as a guideline to assess the capacity of an adsorbent for larger molecules. Therefore, the methylene blue index provides information on the macroporosity of adsorbents [24]. The methylene blue index values of the studied clays are presented in **Table 5**. They remain relatively constant, around 330 $mg{\cdot}g^{-1}$ for all samples. This slight variation suggests a fairly homogeneous distribution of mesopores and external surfaces among the different types of clay studied, regardless of their origin [66]. Furthermore, for all samples, the iodine index values (**Table 5**) are higher than the methylene blue adsorption capacity values. These results indicate a predominance of micropores over macropores in the samples, thus suggesting that the clay materials studied are essentially microporous [64].

Table 5. Adsorption properties.

	Iodine index ($mg{\cdot}g^{-1}$)	Methylene blue index ($mg{\cdot}g^{-1}$)	pH_{pzc}
KR	593.55 ± 0.2	320.21 ± 0.065	6.1 ± 0.1
KB	511.50 ± 0.15	329.54 ± 0.005	5.3 ± 0.2
BB	505.03 ± 0.1	329.99 ± 0.025	5.4 ± 0.2

In comparison with international studies, the adsorption capacities of natural clays vary greatly depending on the mineralogy, applied treatments, and experimental conditions. Some natural clays have shown high performance for methylene blue, reaching 456.6 mg/g in alkaline medium, while purified or activated clays can display even higher values (≈681 - 1383 mg/g), due to an increased specific surface area and cation exchange capacity [67] [68].

Furthermore, the Ivorian clays studied exhibit a high iodine value (~505 - 593 mg/g), indicating well-developed microporosity and an adsorption potential comparable to that of certain potential natural clays. The iodine value values obtained are also comparable to those reported for some natural clays used as adsorbents (500 - 700 mg/g) [25]. However, these values remain lower than those observed for activated clays or activated carbons [25]. From a mineralogical perspective, the presence of smectite in KB could explain its relatively high adsorption potential, as reported in several studies showing that 2:1 clays have a higher adsorption capacity than kaolinites, due to their larger specific surface area and high cation exchange capacity. Furthermore, the iron oxides present in KR could also contribute to the potential for anion adsorption by forming surface complexes, thereby strengthening the mechanisms of interaction with certain pollutants [7] [69].

Such a structure promotes the adsorption of both small molecules and larger organic compounds, thus confirming the potential of the studied clays for a wide range of organic pollutants [70].

4. Conclusion

The physico-chemical, mineralogical, and morphological investigations conducted on the three Ivorian clays (KR, KB, and BB) made it possible to establish clear correlations between their composition and their adsorptive performance. The results show a predominance of kaolinite in KR and BB, whereas KB is characterized by a significant proportion of montmorillonite and illite. The notable presence of goethite, particularly in KR, gives this sample an iron-rich enrichment that could influence surface interaction mechanisms. The adsorptive properties, assessed through iodine and methylene blue indices and the pH at the point of zero charge, reveal variable performances depending on the mineralogical nature and chemical composition. KR exhibits the best micropollutant adsorption capacity, attributed to its richness in active phases and iron oxides. KB also shows an interesting potential, linked to the presence of 2:1 minerals and exchangeable cations that favor ion exchange mechanisms. In contrast, BB, richer in silica and less concentrated in reactive phases, exhibits relatively more moderate performances. These results confirm the potential for valorizing local clay resources in contaminated water treatment processes. The observed differences pave the way for a targeted use of these materials depending on the type of pollutant to be removed. However, physical or chemical activation treatments could be considered to improve their surface properties and optimize their adsorption capacities with a view to larger-scale application.

Conflicts of Interest

The authors declare no conflicts of interest regarding the publication of this paper.

References

[1] Sanou, Y. and Paré, S. (2021) Study of the Adsorptive Power of a Ferrihydrite-Doped Laterite for the Removal of Arsenic (V) from Water. *Journal de la Société Ouest-Africaine de Chimie*, **50**, 41-49.

[2] Sagou, J.-P.S., Kouassi, S.S., Kouakou, L.P.M.-S., Konan, L.K., Andji-Yapi, Y.J. and Allard, T. (2017) Structural Order of Clays from Gounioube's Deposit (Ivory Coast): Study by Electron Paramagnetic Resonance Spectroscopy. *American Journal of Materials Science and Engineering*, **5**, 37-42.

[3] Wang, P., Shen, X., Qiu, S., Zhang, L., Ma, Y. and Liang, J. (2024) Clay-Based Materials for Heavy Metals Adsorption: Mechanisms, Advancements, and Future Prospects in Environmental Remediation. *Crystals*, **14**, Article 1046. https://doi.org/10.3390/cryst14121046

[4] Qi, Y., Zhao, S., Shen, Y., Jiang, X., Lv, H. and Han, C. (2024) A Critical Review of Clay Mineral-Based Photocatalysts for Wastewater Treatment. *Catalysts*, **14**, Article 575. https://doi.org/10.3390/catal14090575

[5] Hacıosmanoğlu, G.G., Mejías, C., Martín, J., Santos, J.L., Aparicio, I. and Alonso, E. (2022) Antibiotic Adsorption by Natural and Modified Clay Minerals as Designer Adsorbents for Wastewater Treatment: A Comprehensive Review. *Journal of Environmental Management*, **317**, Article 115397. https://doi.org/10.1016/j.jenvman.2022.115397

[6] Kouakou, L.P.M., Karidioula, D., Manouan, M.R.W., Pohan, A.G.L., Cissé, G. and Konan, L.K. (2023) Use of Two Clays from Côte d'ivoire for the Adsorption of Methyl Red from Aqueous Medium. *Chemical Physics Letters*, **810**, Article 140183. https://doi.org/10.1016/j.cplett.2022.140183

[7] Ake, A.P., Coulibaly, V., Ouattara, Y.N., Kouadio, L.M., Kouakou, L.P.M. and Aketchi, T.L. (2025) Study of the Influence of Some Ions on the Adsorption of Phosphates by Clay Materials from Côte d'ivoire. *International Research Journal of Pure and Applied Chemistry*, **26**, 96-111. https://doi.org/10.9734/irjpac/2025/v26i2909

[8] Ladjal, N., Terchi, S. and Debih, H. (2024) High Efficiency Adsorption Performance of Basic Dye (Crystal Violet) onto Algerian Montmorillonite. *Studii şi Cercetări Ştiinţifice*, **25**, 1-18.

[9] Puri, C. and Sumana, G. (2018) Highly Effective Adsorption of Crystal Violet Dye from Contaminated Water Using Graphene Oxide Intercalated Montmorillonite Nanocomposite. *Applied Clay Science*, **166**, 102-112. https://doi.org/10.1016/j.clay.2018.09.012

[10] Adegoke, K.A., Adesina, O.O., Okon-Akan, O.A., Adegoke, O.R., Olabintan, A.B. and Ajala, O.A. (2022) Sawdust-Biomass Based Materials for Sequestration of Organic and Inorganic Pollutants and Potential for Engineering Applications. *Current Research in Green and Sustainable Chemistry*, **5**, Article 100274. https://doi.org/10.1016/j.crgsc.2022.100274

[11] Ahmed, M.J., Danish, M., Anastopoulos, I. and Iwuozor, K.O. (2023) Recent Progress on Corn (*Zea mays* L.)-Based Materials as Raw, Chemically Modified, Carbonaceous, and Composite Adsorbents for Aquatic Pollutants: A Review. *Journal of Analytical and Applied Pyrolysis*, **172**, Article 106004. https://doi.org/10.1016/j.jaap.2023.106004

[12] Joseph, A.Y., Martial, A.K.D., Soumahoro, G. and Benjamin, Y.K. (2023) Modelling and Optimization of Simultaneous Removal of Ions (H2PO4-, NO3- and Cd2+) by Adsorption on Clay in Aqueous Solution by Using Response Surface Methodology. *Chemical Science International Journal*, **32**, 51-62. https://doi.org/10.9734/csji/2023/v32i5860

[13] Kedi, A.B.B., Kouassi, S.S., Coulibaly, V. and Sei, J. (2021) Elimination de polluants des déchets liquides d'une unité de production de sucre par des argiles naturelles de Côte d'Ivoire. *International Journal of Biological and Chemical Sciences*, **15**, 803-815. https://doi.org/10.4314/ijbcs.v15i2.31

[14] Coulibaly, Y., Cathelineau, M. and Boiron, M. (2026) Supergene Alteration of Skarn and Marble at Flotouo (Ity, Ivory Coast): Controls on Gold and Trace-Metal Enrichment in the Saprolite. *Minerals*, **16**, Article 162. https://doi.org/10.3390/min16020162

[15] Kouamelan, A.N., Djro, S.C., Allialy, M.E., Paquette, J. and Peucat, J. (2015) The Oldest Rock of Ivory Coast. *Journal of African Earth Sciences*, **103**, 65-70. https://doi.org/10.1016/j.jafrearsci.2014.12.004

[16] N'zi, J.C., Toure, M., Yao, N.J., Kouassi, R.A., Digbehi, Z.B. and Aka, K. (2018) Caracterisation sedimentologique et mineralogique des formations tertiares du bassin onshore de la region d'abidjan, Cote d'Ivoire. *European Scientific Journal, ESJ*, **14**, Article 218. https://doi.org/10.19044/esj.2018.v14n18p218

[17] Bishweka, C., Manjia, M.B., Ngapgue, F., Nana, U.J.M.P. and Pettang, C. (2021) Contribution to the Characterization of Lateritic Soils for the Manufacture of Compressed Stabilized Earth Bricks. *Open Journal of Civil Engineering*, **11**, 411-426. https://doi.org/10.4236/ojce.2021.114024

[18] Et-Tayea, Y., Harrati, A., Rachid, A., Nasri, H., Attou, A. and Arkame, Y. (2023) Mineralogical and Physico-Chemical Characterization of Bentonite Materials from the Oued Zemmour Area (Oriental Rif, Nador-Morocco): Valorization in Ceramic Field. *Boletín de la Sociedad Española de Cerámica y Vidrio*, **62**, 268-283. https://doi.org/10.1016/j.bsecv.2022.03.001

[19] Nshimiyimana, P., Fagel, N., Messan, A., Wetshondo, D.O. and Courard, L. (2020) Physico-chemical and Mineralogical Characterization of Clay Materials Suitable for Production of Stabilized Compressed Earth Blocks. *Construction and Building Materials*, **241**, Article 118097. https://doi.org/10.1016/j.conbuildmat.2020.118097

[20] Khireddine, O. (2016) Étude de matériaux argileux et leur Impact sur l'adsorption de cer-tains polluants. Ph.D. Thesis, Université Badji Mokhtar Annaba.

[21] Staljanssens, M. (1975) Destruction de la matière organique par calcination à basse température en vue de l'analyse minéralogique des sols. *Annales de la Société Géologique de Belgique*, **98**, 393-403.

[22] Laibi, A.B., Gomina, M., Sorgho, B., Sagbo, E., Blanchart, P. and Boutouil, M. (2017) Physicochemical and Geotechnical Characterization of Two Clayey Sites in Benin with a View to Their Valorization in Eco-Construction. *International Journal of Biological and Chemical Sciences*, **11**, Article 499. https://doi.org/10.4314/ijbcs.v11i1.40

[23] Gagea, L. and Mirica, E. (1998) Chimia fizica si ingineria sistemelor oxidice. *QUO VADIS*, Cluj-Napoca, 190 p.

[24] Djonga, W.G., Noubissié, E. and Noumi, G.B. (2019) Discoloration Test of a Slaughterhouse Effluent by Adsorption on Two Adsorbents Produced from Sawdust of Khaya Senegalensis and Pinus Sp. *Results in Engineering*, **4**, Article 100068. https://doi.org/10.1016/j.rineng.2019.100068

[25] Nwosu, F.O., Ajala, O.J., Owoyemi, R.M. and Raheem, B.G. (2018) Preparation and Characterization of Adsorbents Derived from Bentonite and Kaolin Clays. *Applied Water Science*, **8**, Article No. 195. https://doi.org/10.1007/s13201-018-0827-2

[26] Bestani, B., Benderdouche, N., Benstaali, B., Belhakem, M. and Addou, A. (2008) Methylene Blue and Iodine Adsorption onto an Activated Desert Plant. *Bioresource Technology*, **99**, 8441-8444. https://doi.org/10.1016/j.biortech.2008.02.053

[27] Mahamane, N.A.K, Fanou, G.D., Konan, A.T.S., Ouattara, A., Kone, H., Malam, A.M.M., Assidjo, E.N. and Yao, K.B. (2022) Process Conditions Optimization of Plant Waste-Derived Microporous Activated Carbon Using a Full Factorial Design and Genetic Algorithm. *Journal of Materials and Environmental Science*, **13**, 884-899.

[28] Gee, G.W. and Or, D. (2002) 2.4 Particle-Size Analysis. In: Dane, J.H. and Clarke Topp, G., Éd., *SSSA Book Series*, 1re Edition, Vol. 5, Wiley, 255-293.

[29] Wang, Y., Li, K., Li, J. and Tang, S. (2021) Influence of Soil Particle Size on the Engineering Properties and Microstructure of a Red Clay. *Applied Sciences*, **11**, Article 10887. https://doi.org/10.3390/app112210887

[30] Sanou, I. (2017) Influence du mélange ciment-pouzzolane sur quelques propriétés phy-siques et mécaniques des adobes. Ph.D. Thesis, Université Joseph Ki-Zerbo.

[31] Sorgho, B. (2013) Caractérisation et valorisation de quelques argiles du Burkina Faso: Application au traitement des eaux et aux géomatériaux de construction. Ph.D. Thesis, Université de Ouagadougou.

[32] Bodian, S., Faye, M., Sambou, V., Séne, N.A., Diaw, I. and Faye, K. (2021) Caractérisation physico-chimique des matières premières argileuses de la carrière de thicky (sénégal) pour la fabrication de briques en terre. *Journal de Physique de la Soaphys*, **3**, 1-7. https://doi.org/10.46411/jpsoaphys.2021.01.01

[33] Almasoudi, R., Abuel-Naga, H. and Daghistani, F. (2023) Effects of Dry Density and Moisture Content on the Kaolin-Brass Interfacial Shear Adhesion. *Applied Sciences*, **13**, Article 11191. https://doi.org/10.3390/app132011191

[34] Deon, F., van Ruitenbeek, F., van der Werff, H., van der Meijde, M. and Marcatelli, C. (2022) Detection of Interlayered Illite/Smectite Clay Minerals with XRD, SEM Analyses and Reflectance Spectroscopy. *Sensors*, **22**, Article 3602. https://doi.org/10.3390/s22093602

[35] Ewis, D., Ba-Abbad, M.M., Benamor, A. and El-Naas, M.H. (2022) Adsorption of Organic Water Pollutants by Clays and Clay Minerals Composites: A Comprehensive Review. *Applied Clay Science*, **229**, Article 106686. https://doi.org/10.1016/j.clay.2022.106686

[36] Campillo-Cora, C., Conde-Cid, M., Arias-Estévez, M., Fernández-Calviño, D. and Alonso-Vega, F. (2020) Specific Adsorption of Heavy Metals in Soils: Individual and Competitive Experiments. *Agronomy*, **10**, Article 1113. https://doi.org/10.3390/agronomy10081113

[37] Coulibaly, S.L. (2014) Abattement des phosphates des eaux usées par adsorption sur des géomatériaux constitués de Latérite, grès et schistes ardoisiers. Ph.D. Thesis, L'Université de Lorraine (UL) et de L'Université Nangui Abrogoua (UNA).

[38] Sako, I., Kouamé, A.N., Ossonon, D.B., Kinimo, K.C. and Goure Doubi, B.I.H. (2025) Evaluation of the Physico-Chemical Properties of Two Clays for Use as Adsorbents in Wastewater Treatment. *Journal of Materials and Environmental Science*, **16**, 1709-1720.

[39] Konan, K.L. (2006) Interactions entre des matériaux argileux et un milieu basique riche en calcium. Ph.D. Thesis, Université de Limoges.

[40] Zhang, B., Yu, T., Guo, H., Chen, J., Liu, Y. and Yuan, P. (2022) Effect of the SiO_2/Al_2O_3 Molar Ratio on the Microstructure and Properties of Clay-Based Geopolymers: A Comparative Study of Kaolinite-Based and Halloysite-Based Geopolymers: A Comparative Study of Kaolinite-based and Halloysite-Based Geopolymers. *Clays and Clay Minerals*, **70**, 882-902. https://doi.org/10.1007/s42860-023-00223-x

[41] Marco-Brown, J.L., Guz, L., Olivelli, M.S., Schampera, B., Torres Sánchez, R.M. and Curutchet, G. (2018) New Insights on Crystal Violet Dye Adsorption on Montmorillonite: Kinetics and Surface Complexes Studies. *Chemical Engineering Journal*, **333**, 495-504. https://doi.org/10.1016/j.cej.2017.09.172

[42] Tejeogue, J.P.N., Djakba, R., Fotsop, C.G., Dobe, N., Mouhamadou, S. and Wangmene, B. (2025) Systematic Metronidazole Adsorption Performance onto Montmorillonite Clay: Parametric Study, Process Modelling and RSM Optimisation. *Results in Chemistry*, **14**, Article 102153. https://doi.org/10.1016/j.rechem.2025.102153

[43] Mao, X., Liu, H., Chu, Z., Chen, T., Zou, X. and Chen, D. (2022) Adsorption of Lead by Kaolinite, Montmorillonite, Goethite and Ferrihydrite: Performance and Mechanisms Based on Quantitative Analysis. *Clay Minerals*, **57**, 230-240. https://doi.org/10.1180/clm.2022.41

[44] Kang, J., Li, J., Ma, C., Yi, L., Gu, T. and Wang, J. (2022) Goethite/Montmorillonite Adsorption Coupled with Electrocoagulation for Improving Fluoride Removal from Aqueous Solutions. *RSC Advances*, **12**, 7475-7484. https://doi.org/10.1039/d1ra08503d

[45] Adebayo, G.B., Adegoke, H.I. and Fauzeeyat, S. (2020) Adsorption of Cr(vi) Ions onto Goethite, Activated Carbon and Their Composite: Kinetic and Thermodynamic Studies. *Applied Water Science*, **10**, Article No. 213. https://doi.org/10.1007/s13201-020-01295-z

[46] Zango, Z.U., Garba, A., Garba, Z.N., Zango, M.U., Usman, F. and Lim, J. (2022) Montmorillonite for Adsorption and Catalytic Elimination of Pollutants from Wastewater: A State-of-the-Arts Review. *Sustainability*, **14**, Article 16441. https://doi.org/10.3390/su142416441

[47] Bakary Soro, S., Coulibaly, M., Paul Gauly, L., N'Dri, S.R., Sanou, A. and Trokourey, A. (2023) Characterization of Clay Materials from Côte d'ivoire: Possible Application for the Electrochemical Analysis. *Journal of Materials Science Research*, **12**, Article 51. https://doi.org/10.5539/jmsr.v12n1p51

[48] Fort, C.I., Sanou, A., Coulibaly, M., Yao, K.B. and Turdean, G.L. (2024) Green Modified Electrode for Sensitive Simultaneous Heavy Metal Ions Electrodetection. *Sensors and Actuators B: Chemical*, **418**, Article 136326. https://doi.org/10.1016/j.snb.2024.136326

[49] Gauly, L.P., Coulibaly, M., Soro, S.B., Kouadio, K.S., N'Dri, S.R. and Sanou, A. (2025) Characterization and Enhanced Performance of Ivorian Clays as Potential Modifiers in Carbon Paste Electrodes. *Discover Applied Sciences*, **7**, Article No. 128. https://doi.org/10.1007/s42452-024-06457-1

[50] Taïpabé, D., Doko, K.V., Datchossa, T.A., Abdourahamane, A.I., Mandela, T., Sanou A. and Gibigaye, M. (2025) Characterization of a Lateritic Soil in Chad with a View to Its Use in Ecoconstruction. *Journal of Materials and Environmental Science*, **16**, 1189-1209.

[51] Konan, K.L., Soro, J., Andji, J.Y.Y., Oyetola, S. and Kra, G. (2010) Etude comparative de la déshydroxylation/amorphisation dans deux kaolins de cristallinité différente. *Journal de la Société Ouest-Africaine de Chimie*, **30**, 29-39.

[52] Taïpabé, D., Doko, K.V., Datchossa, T.A., Bozabé, R.K. and Gibigaye, M. (2025)

Physic Mechanical Behaviours of Raw Earth Bricks: Case of Laterite Stabilized with Gum Arabic and Reinforced with Sugarcane Bagasse in Chad. *Open Journal of Civil Engineering*, **15**, 56-69. https://doi.org/10.4236/ojce.2025.151004

[53] Böhm, L., Grančič, P., Scholtzová, E., Heyde, B.J., Düring, R. and Siemens, J. (2022) Adsorption of the Hydrophobic Organic Pollutant Hexachlorobenzene to Phyllosilicate Minerals. *Environmental Science and Pollution Research*, **30**, 36824-36837. https://doi.org/10.1007/s11356-022-24818-4

[54] Dao, K., Ouedraogo, M., Millogo, Y., Aubert, J. and Gomina, M. (2018) Thermal, Hydric and Mechanical Behaviours of Adobes Stabilized with Cement. *Construction and Building Materials*, **158**, 84-96. https://doi.org/10.1016/j.conbuildmat.2017.10.001

[55] Sanou, A., Coulibaly, M., N'dri, S.R., Tămaș, T.L., Bizo, L. and Frentiu, T. (2024) Raw Clay Material-Based Modified Carbon Paste Electrodes for Sensitive Heavy Metal Detection in Drinking Water. *Journal of Materials Science*, **59**, 13961-13977. https://doi.org/10.1007/s10853-024-09945-2

[56] Konan, K.L., Sei, J., Soro, N.S., Oyetola, S., Gaillard, J.M., Bonnet, J.P. and Kra, G. (2006) Caractérisation de matériaux argileux du site d'Azaguie-Blida (Anya-ma, Côte d'Ivoire) et détermination des propriétés mécaniques de produits céramiques. *Journal de la Société ouest-africaine de chimie*, **21**, 35-43.

[57] Méité, N., Konan, L.K., Tognonvi, M.T., Doubi, B.I.H.G., Gomina, M. and Oyetola, S. (2021) Properties of Hydric and Biodegradability of Cassava Starch-Based Bioplastics Reinforced with Thermally Modified Kaolin. *Carbohydrate Polymers*, **254**, Article 117322. https://doi.org/10.1016/j.carbpol.2020.117322

[58] Ptáček, P., Frajkorová, F., Šoukal, F. and Opravil, T. (2014) Kinetics and Mechanism of Three Stages of Thermal Transformation of Kaolinite to Metakaolinite. *Powder Technology*, **264**, 439-445. https://doi.org/10.1016/j.powtec.2014.05.047

[59] Drits, V.A., Zviagina, B.B., Sakharov, B.A., Dorzhieva, O.V. and Savichev, A.T. (2021) New Insight into the Relationships between Structural and Ftir Spectroscopic Features of Kaolinites. *Clays and Clay Minerals*, **69**, 366-388. https://doi.org/10.1007/s42860-021-00133-w

[60] Aké, A.P., Coulibaly, V., Kouamé, N., Kedi, A.B., Sei, J. and Oyetola, S. (2022) Study of the Status of Iron in Clay Materials from Côte d'Ivoire for Their Use as Phosphate Adsorbents. *RAMRES Sciences des Structures et de la Matière*, **6**, 63-90.

[61] Sore, S.O., Nshimiyimana, P., Messan, A., Prud'homme, E., Tsobnang, F. and Escadeillas, G. (2025) Chemical and Mineralogical Characterizations of Different Kaolinitic Clays from Burkina Faso: Feasibility for the Synthesis of Geopolymer Binders. *Geosciences*, **15**, Article 230. https://doi.org/10.3390/geosciences15060230

[62] Yapo, N.S., Briton, B.G.H., Aw, S., Reinert, L., Drogui, P. and Adouby, K. (2021) Bivalve Shells (*Corbula trigona*) as a New Adsorbent for the Defluoridation of Groundwater by Adsorption-precipitation. *Journal of Environmental Science and Health, Part A*, **56**, 694-704. https://doi.org/10.1080/10934529.2021.1917937

[63] Wijeyawardana, P., Nanayakkara, N., Gunasekara, C., Karunarathna, A., Law, D. and Pramanik, B.K. (2022) Removal of Cu, Pb and Zn from Stormwater Using an Industrially Manufactured Sawdust and Paddy Husk Derived Biochar. *Environmental Technology & Innovation*, **28**, Article 102640. https://doi.org/10.1016/j.eti.2022.102640

[64] Konan, A. (2019) Couplage adsorption-procédés d'oxydation avancée pour l'élimination de polluants biorécalcitrants en milieu aqueux. Ph.D. Thesis, Université de Toulouse/Institut National Polytechnique Félix Houphouët-Boigny.

[65] Raposo, F., De La Rubia, M.A. and Borja, R. (2009) Methylene Blue Number as Useful Indicator to Evaluate the Adsorptive Capacity of Granular Activated Carbon in Batch Mode: Influence of Adsorbate/adsorbent Mass Ratio and Particle Size. *Journal of Hazardous Materials*, **165**, 291-299. https://doi.org/10.1016/j.jhazmat.2008.09.106

[66] Varlikli, C., Bekiari, V., Kus, M., Boduroglu, N., Oner, I. and Lianos, P. (2009) Adsorption of Dyes on Sahara Desert Sand. *Journal of Hazardous Materials*, **170**, 27-34. https://doi.org/10.1016/j.jhazmat.2009.05.030

[67] Loutfi, M., Mariouch, R., Mariouch, I., Belfaquir, M. and ElYoubi, M.S. (2023) Adsorption of Methylene Blue Dye from Aqueous Solutions onto Natural Clay: Equilibrium and Kinetic Studies. *Materials Today*: *Proceedings*, **72**, 3638-3643. https://doi.org/10.1016/j.matpr.2022.08.412

[68] Ouaddari, H., Abbou, B., Lebkiri, I., Habsaoui, A., Ouzzine, M. and Fath Allah, R. (2024) Removal of Methylene Blue by Adsorption onto Natural and Purified Clays: Kinetic and Thermodynamic Study. *Chemical Physics Impact*, **8**, Article 100405. https://doi.org/10.1016/j.chphi.2023.100405

[69] Kouadio, L.M., Lebouachera, S.E.I., Blanc, S., Sei, J., Miqueu, C. and Pannier, F. (2022) Characterization of Clay Materials from Ivory Coast for Their Use as Adsorbents for Wastewater Treatment. *Journal of Minerals and Materials Characterization and Engineering*, **10**, 319-337. https://doi.org/10.4236/jmmce.2022.104023

[70] Massesse-Loudi, M., Boukongou, A., Mongo, D. and Barhé, T. (2025) Study of the Adsorption of Difenoconazole on Char in Aqueous Medium. *American Journal of Chemical Engineering*, **13**, 14-19. https://doi.org/10.11648/j.ajche.20251301.12